International Journal of Heat and Mass Transfer 52 (2009) 2255–2264

Contents lists available at ScienceDirect

International Journal of Heat and Mass Transfer

journal homepage: www.elsevier.com/locate/ijhmt

Temperature amplification during laser heating of polycrystalline silicon microcantilevers due to temperature-dependent optical properties

Justin R. Serrano [a], Leslie M. Phinney [a,*], James W. Rogers [b]

[a] Engineering Sciences Center, Sandia National Laboratories, Albuquerque, NM 87185-0346, USA
[b] Department of Engineering and Physics, Murray State University, Murray, KY 42071, USA

ARTICLE INFO

Article history:
Received 29 May 2008
Received in revised form 28 October 2008
Available online 3 February 2009

Keywords:
MEMS
Optical absorption
Polysilicon
Raman thermometry
Thermal model

ABSTRACT

The absorption of optical energy and subsequent thermal transport are investigated experimentally and numerically for 500 μm long, 250 μm wide, and 2.25 μm thick polycrystalline silicon microcantilevers irradiated by an 808 nm continuous-wave laser. Temperature profiles were measured using Raman thermometry at 314 and 532 mW of laser power, and the microcantilever peak temperature was measured for laser powers up to 719 mW. A modular technique for multilayered structures is used to calculate the optical absorption in polysilicon microcantilevers, and the thermal response is then calculated with a two-dimensional, finite difference model. Very good agreement is obtained between the measured and calculated temperature profiles and peak temperatures versus laser power. The abrupt increase or amplification of peak temperature for laser powers between 415 and 440 mW is shown to be a result of peaks in the temperature-dependent optical absorptance.

1. Introduction

Lasers are broadly utilized in microelectromechanical systems (MEMS) applications as integral components in optical devices, as displacement detectors, and as fabrication tools in MEMS processing. For some optical MEMS devices, laser irradiation is integral to their functionality. Optical MEMS applications include projection displays, optical switches, adaptive optics, optical cross-connects, and laser powered thermal actuators. Microsystems irradiated with a laser overheat when the laser power levels exceed the thermal management capabilities of the device resulting in permanent deformation and damage [1–6]. The ability to model numerically the behavior of MEMS components heated with a laser furthers the understanding of the physical phenomena, aids in establishing processing parameters, and facilitates optical MEMS design, optimization, and failure analysis [7–9].

The thermal response of a microdevice irradiated by a laser depends on the amount of optical energy that is absorbed and the subsequent thermal transport within the microstructure. The absorption of optical energy is determined by the optical properties of the material, geometry of the structure, and laser wavelength. The thicknesses of surface-micromachined MEMS range from one to tens of microns, which is on the same order as the optical penetration depth for infrared laser wavelengths. Thus, interference affects the optical response when the constituent material is partially transparent at the laser wavelength. Polycrystalline silicon (polysilicon) is a typical structural material in surface micromachining processes and has optical penetration depths of a few microns for wavelengths in the red and near infrared. For these reasons, the optical absorption of infrared lasers in polysilicon MEMS is very sensitive to the thicknesses of the structures and underlying gaps. Also, the temperature dependence of the optical properties impacts the absorption of laser energy. Recently, spatially resolved temperature profiles were measured on polysilicon microcantilevers and laser-heated microthermal actuators using micro-Raman thermometry [6,10]. In certain regimes, the MEMS parts exhibited sharp increases in temperature in response to a relatively small increase in incident laser power. This type of thermal response needs further study as abrupt increases or amplification of the temperature could lead to sudden overheating and device damage.

In order to develop confidence in numerical modeling results, it is necessary to validate these results with experimental data. Using test structures with straightforward geometries simplifies comparisons between numerical and experimental studies. This paper reports on an investigation of the absorption of incident laser energy and the thermal response of polysilicon microcantilevers heated with 808 nm laser irradiation. Raman thermometry was used to measure the temperature for laser-heated polysilicon microcantilevers, and the optical response of the microcantilever is calculated using a modular technique for obtaining the absorptance within a multilayer structure. A two-dimensional, explicit, finite difference model was developed to compute the temperatures in a laser-heated microcantilever which are compared to the experimental

* Corresponding author. Tel.: +1 505 845 8484; fax: +1 505 844 6620.
E-mail address: lmphinn@sandia.gov (L.M. Phinney).

0017-9310/$ - see front matter © 2008 Elsevier Ltd. All rights reserved.
doi:10.1016/j.ijheatmasstransfer.2008.12.003

Nomenclature

C	heat capacity (J/m^3 K)
Fo	Fourier number
h	heat transfer coefficient (W/m^2 K)
I	laser intensity (W/m^2)
I_0	peak laser intensity (W/m^2)
k	thermal conductivity of cantilever (W/m K)
k_{air}	thermal conductivity of air (W/m K)
L_{imag}	distance to imaginary surface used for convection model (μm)
S	laser source term (W/m^2)
T	temperature (°C)
T_0	reference temperature (°C)
T_∞	air temperature (°C)
t	time (s)
Δt	time step (s)
t_{gap}	gap between bottom of cantilever and substrate (μm)
w_x	laser spot $1/e^2$ radius in x-direction (μm)
w_y	laser spot $1/e^2$ radius in y-direction (μm)
x	distance along length of cantilever (μm)
x_0	location of center of laser beam in x-direction (μm)
Δx	spatial step between nodes in both x- and y-directions (μm)
y	distance along width of cantilever (μm)
y_0	location of center of laser beam in y-direction (μm)
z	Thickness of cantilever (μm)
N	real part of refractive index
K	imaginary part of refractive index
FWHM	full width at half maximum

Greek

α	absorptance coefficient
Ω	Raman peak position
Ω_0	Raman peak position at T_0

Subscripts and superscripts

m	node in x-direction
n	node in y-direction
p	time step
580poly	corresponding to polysilicon deposited at 580 °C
605poly	corresponding to polysilicon deposited at 605 °C
630poly	corresponding to polysilicon deposited at 630 °C
Si	corresponding to bulk silicon

results. The modeling and simulation results provide insight into the phenomena resulting in temperature amplification as the laser power is increased.

2. Microcantilever design and fabrication

Polysilicon cantilever test structures were fabricated from the fourth structural layer, Poly4, in the five-layer polysilicon surface micromachining process, SUMMiT™V (Sandia Ultra-planar Multi-level MEMS Technology) [11]. The SUMMiT™V process uses four structural polysilicon layers with a fifth layer as a ground plane [11]. Each layer is separated by sacrificial oxide layers that are etched away during the final release step. The highest two structural layers, Poly3 and Poly4, are nominally 2.25 μm in thickness, while the lower two, Poly1 and Poly2, are nominally 1.0 μm and 1.5 μm in thickness, respectively. The ground plane, Poly0, is 300 nm in thickness and is deposited above an 800 nm layer of silicon nitride and a 630 nm layer of SiO_2. The sacrificial oxide layers between the structural layers are each 2.0 μm thick.

Fig. 1 shows a polysilicon Poly4 microcantilever used in this study. The microcantilever is 250 μm wide, 500 μm long, and 2.25 μm thick. Release etch holes are 4 μm by 4 μm and distributed in a 25 μm by 25 μm grid pattern on the cantilever. The gap between the bottom of the cantilever and the substrate is nominally 10.75 μm. The distance under a Poly4 structure varies by ±0.25 μm due to process variations.

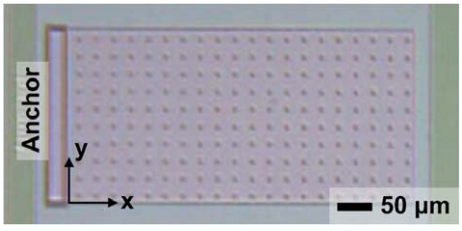

Fig. 1. Image of a 250 μm wide, 500 μm long, and 2.25 μm thick polysilicon microcantilever. The axes indicate the origin for the numerical calculations.

3. Raman thermometry and temperature measurements

The samples in this study were irradiated with a fiber-coupled, continuous-wave (CW) diode laser with a wavelength of 808 nm and adjustable power. A schematic diagram of the experimental setup is shown in Fig. 2. The output from the laser was focused on the sample through a 100 μm core diameter multimode fiber that was coupled to a 1:1 relay lens. The relay lens is mounted on an $XYZ\theta$ stage that permits four degrees of movement of the fiber. The laser delivery stage was designed specifically to operate within the physical constraints imposed by the imaging optics of the Raman microscope. These limitations required the use of an oblique irradiation angle that could be varied between ~50° and 75° from the normal direction and which also had sufficient working distance to not interfere with the objective lens assembly of the Raman microscope. For the tests discussed in this paper, the lens was mounted at 60° to the *Z-direction* (30° to the *XY-plane)* which results in a 210 μm × 106 μm (FWHM) elliptical spot on the surface. These dimensions are very convenient for the experiments discussed here. The beam intensity at the sample position can be approximated by a Gaussian-like profile with the stated

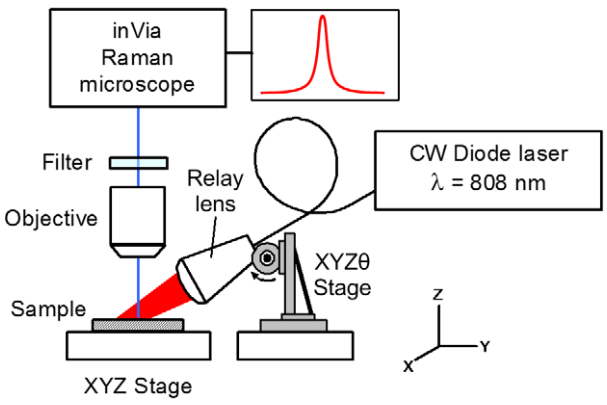

Fig. 2. Experimental layout for simultaneous irradiation and thermometry of MEMS structures.

widths measured at the half-intensity points along both axes. The relay lens stage is mounted on a second *XYZ* stage which holds the sample under the microscope used to collect the Raman spectra. An IR cutoff filter is placed behind the microscope objective to prevent any scattered infrared light from obscuring the Raman signal.

Raman measurements were taken in a Renishaw inVia Raman microscope that uses a 180° backscattering geometry and a 488 nm Ar^+ laser as the probe. When combined with a 20×, 0.42 numerical aperture (NA) objective, the spatial resolution for the measurements is better than 1.5 μm. For thermometry purposes, different temperature-induced changes to the Raman spectrum from the sample can be used as temperature metrics [12–16]. For this study, only the peak position of the Stokes Raman peak for polysilicon was used for diagnostics. This metric is a very reliable thermometer in the absence of evolving in-plane stresses [14–15]. Through a calibration procedure on a polysilicon film heated in a temperature-controlled hot stage, the response of the Raman peak position, Ω, was found to be linear with temperature between 25 °C and 700 °C. The temperature of the probed surface can then be determined from the peak position, Ω, through the formula

$$T = T_0 + \left(\frac{d\Omega}{dT}\right)^{-1}(\Omega - \Omega_0) \quad (1)$$

where the slope $d\Omega/dT = -0.024 \pm 0.00016\ \mathrm{cm^{-1}/°C}$ [15,16], and Ω_0 is the peak position measured at temperature T_0 prior to heating the device. It should be noted that the linear dependence observed for polysilicon is only valid over the calibrated temperature range; the relationship is not necessarily linear for other materials or for polysilicon at much lower temperatures [13]. The uncertainty in the temperature measurement obtained with this method, in the absence of evolving in-plane stresses, is less than ±4 °C. For our test structures which are free to expand, the heating is not expected to cause a significant generation of stress to introduce additional uncertainty in the measurement.

To obtain temperature profiles of the laser-heated surfaces, Raman spectra were collected at 20 μm intervals along the sample surface. At each position, five spectra were taken with a collection time of between 60 and 120 s each. In addition, to avoid introducing bias into the temperature measurement, the probe laser power was reduced to less than 100 μW. Each spectrum collected is fitted to a combined Gaussian–Lorentzian function to permit an accurate determination of the peak position. The average peak position of the five spectra is then converted to temperature using Eq. (1), and the reported uncertainty of ±4 °C reflects the typical variation in the five peak positions.

Irradiation powers used during the testing of the MEMS structures were chosen to remain below the damage thresholds for the structures [2,6,8]. Moreover, because of the long data collection time required for the measurements, the powers were reduced even further to prevent any damage after prolonged exposure to the laser irradiation [2,6]. This is necessary because the Raman thermometry technique requires steady-state thermal conditions while collecting a temperature profile, a measurement process that takes several hours. Temperature measurements were taken for microcantilevers during irradiation with 314 and 532 mW of heating laser power. The 500 μm × 250 μm microcantilevers (cf. Fig. 1) were irradiated at a 60° angle with the elliptical spot centered on the plate surface and the major axis of the spot aligned with the long axis of the cantilever (*x*-axis in Fig. 1). Measured thermal profiles are shown in Figs. 3 and 4 and compared to the results of a thermal model. The model results in Figs. 3–5 are discussed in the thermal modeling section of this article.

For both incident powers, the highest temperature occurred in the center of the irradiated region, with a peak temperature of ~115 °C at 314 mW and ~460 °C at 532 mW. Along the minor axis, the profile is very symmetric, with a pronounced increase in temperature inside irradiated region as shown in Fig. 3b. Along the major axis (Figs. 3a and 4), the differences in the boundary conditions of the two ends are clearly evident. While the temperature decreases away from the center of the irradiated spot, the side closest

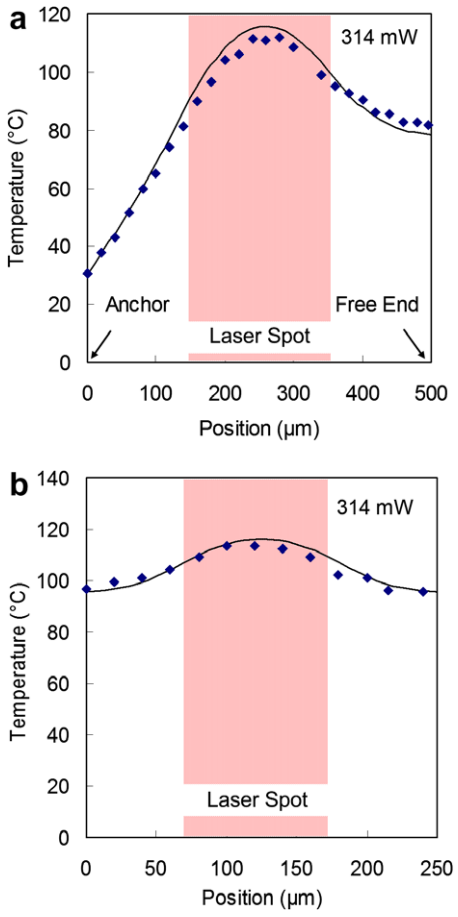

Fig. 3. Temperature profile for a laser-heated cantilever along the (a) central length and (b) central width of the microcantilever when irradiated with 314 mW of laser power. The shaded area indicates the location of the heating laser spot. Experiment (diamonds) and model (line) results are in very good agreement, with an $R^2 = 0.9634$ for the profile along the cantilever length.

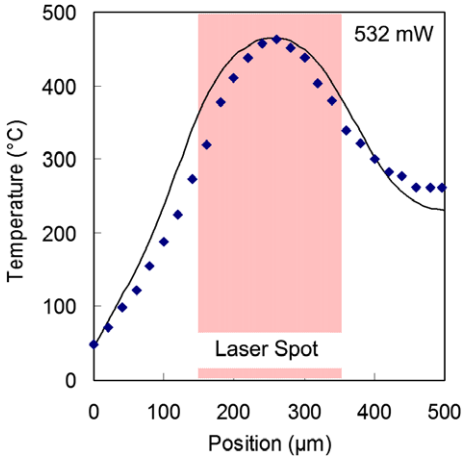

Fig. 4. Temperature profile for a laser-heated cantilever along the central length of the cantilever when irradiated with 532 mW of laser power. The agreement between the experiment (diamonds) and model (line) is not as good ($R^2 = 0.9134$) as at the lower laser power.

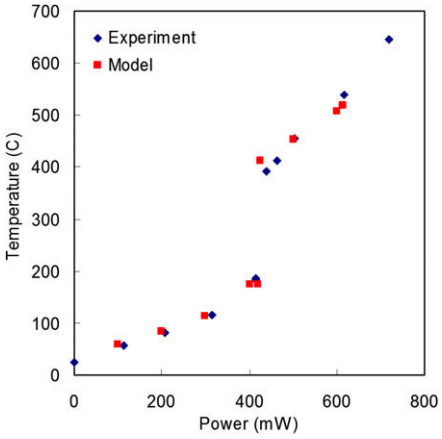

Fig. 5. Peak cantilever temperature as a function of applied laser power for the model (squares) and experiment (diamonds). Excellent agreement between model and experiment exists with the model predicting a jump in peak temperature from 175 to 413 °C with a power increase of just 5 mW from 420 to 425 mW which is consistent with the experimental observations.

to the anchor shows a sharp decrease towards the substrate temperature, while on the free end, the decrease is less pronounced. Interestingly, the results reveal that the assumption of an adiabatic free end, commonly used when modeling extended surfaces is perfectly valid. At both powers, the irradiated region is hotter than the surrounding region which indicates poor thermal transport out of the irradiated region.

The peak temperature at the center of the irradiated region was also investigated as a function of incident laser power. Although the peak temperature is expected to scale linearly with the incident laser power, the results shown in Fig. 5, indicate another mechanism is affecting the thermal behavior of the irradiated plate. The measured temperature increases linearly with power up to a temperature of ~120 °C for incident powers below ~320 mW. A non-linear increase with power is evident as the incident power approaches 440 mW. At a power of 440 mW, the temperature increases abruptly to ~400 °C and then increases linearly up to a temperature of ~650 °C at 719 mW.

4. Optical absorption

For laser-irradiated MEMS, the thermal behavior of an irradiated structure is strongly tied to its absorptance and, therefore, to the temperature and wavelength-dependent optical properties of the target material. The link between the two becomes even more pronounced in a system such as the one discussed here. The complex index of refraction of polysilicon has a strong dependence on temperature [17,18]. Furthermore, at near IR wavelengths, the optical penetration depth is comparable to the thickness of the irradiated layers, such that interference, caused by multiple reflections from interfaces, can create strong variations in absorptance with temperature. To carry out predictive simulations of the thermal behavior of laser-heated, multilayered MEMS structures, it then becomes critical to understand the relationship between the absorption of optical power and the surface temperature.

To assess the optical performance of the structure in this study, a modular technique is used to calculate the optical response of multilayered structures. This technique, adapted from the LTR method proposed by Mazilu et al. [19] for calculating thin film interference effects, permits the extraction of absorptance values for the individual layers in a multilayered structure. In addition, temperature-dependent optical constants of different layers can easily be considered with this technique by carrying out the calculations for different temperature conditions. To apply this method

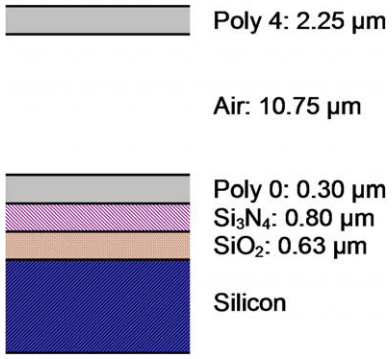

Fig. 6. Layer cross section for SUMMiT™V cantilever used in optical modeling.

to the cantilever structure of this study, a multilayer stack was considered as shown in Fig. 6, and assumed to be irradiated at a 60° angle with an 808 nm source to reflect the conditions of the experiments. The calculations therefore include the interference effects of all the layers in the actual cantilever structure, including the oxide, nitride and air layers under the cantilever. The nominal thicknesses of SUMMiT™V fabricated layers were used for the layer thicknesses and for establishing the proper gap height under the cantilever structure. Because the optical properties of CVD-deposited polysilicon can have strong variations with deposition conditions [17] for polysilicon between room temperature and 1100 °C, several temperature dependencies for the complex index of refraction of the active polysilicon layer were used. The indices correspond to temperature dependencies described in [17] but applied to room-temperature values of the refractive index of SUMMiT™V polysilicon. The functional forms of these dependencies are given in Eq. (2) and are plotted in Fig. 7:

$$N_{Si} = 3.545 + 4.9 \times 10^{-4}(T - T_0);$$
$$K_{Si} = 6.538 \times 10^{-3} \exp((T - T_0)/498) \quad (2a)$$

$$N_{580poly} = 3.545 + 4.3 \times 10^{-4}(T - T_0);$$
$$K_{580poly} = 6.538 \times 10^{-3} \exp((T - T_0)/608) \quad (2b)$$

$$N_{605poly} = 3.545 + 3.56 \times 10^{-4}(T - T_0);$$
$$K_{605poly} = 6.538 \times 10^{-3} \exp((T - T_0)/636) \quad (2c)$$

$$N_{630poly} = 3.545 + 4.43 \times 10^{-4}(T - T_0);$$
$$K_{630poly} = 6.538 \times 10^{-3} \exp((T - T_0)/680) \quad (2d)$$

where T_0 = 20 °C. The thin film interference calculations were then carried out for temperatures from 30 to 600 °C, and assuming that only the top-most layer in the stack undergoes the temperature excursion. From these calculations, the absorbance of the irradiated layer was extracted as a function of temperature, as shown in Fig. 8.

The most significant implication of the temperature excursion of the top-most layer in the optical stack is the presence of a peak in the optical absorptance within this layer as a function of temperature. This peak, which is noted for all temperature dependencies, results from interference caused by the compounding of the reflections from the multiple interfaces and the increase in the index of refraction of the heated surface. As the temperature increases, the optical path length of the laser irradiation within the polysilicon layer changes leading to maxima and minima in the absorption of laser power. The overall change is very pronounced, increasing from ~15% to over 60% over a 200° range for nominal layer thicknesses. Another finding from the calculations is that the location, width, and amplitude of the peak are dependent on the dimensions

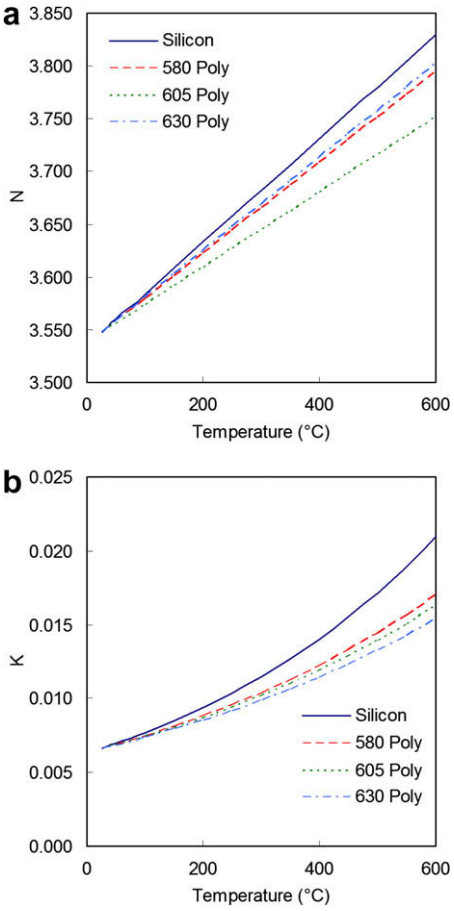

Fig. 7. Real (a) and imaginary (b) part of the complex index of refraction of SUMMiT Poly4 as a function of temperature, at a wavelength of 808 nm, using the different temperature dependencies in Eq. (12).

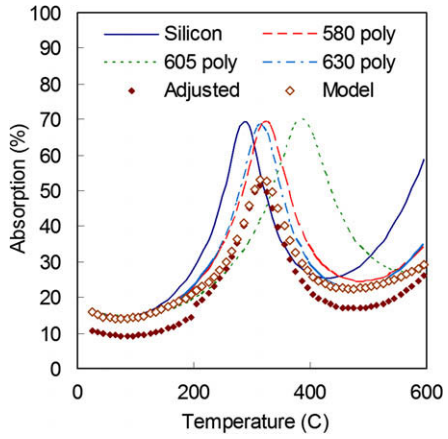

Fig. 8. Absorptance profiles for the multilayered stack in Fig. 6 calculated using nominal dimensions and the different temperature-dependent refractive indices in Eq. (2) (lines). Open symbols represent the absorptance profile calculated for non-nominal dimensions. Closed symbols represent an adjusted profile used in the thermal model calculations.

of the heated film and the underlying gap, with the former having the greatest impact. The open symbols in Fig. 8 show the absorptance profile obtained by varying the dimensions slightly from the nominal values (Poly4 thickness of 2.245 μm and gap height of 10.801 μm), changing the incident angle to 58.7°, and using the optical properties in Eq. (2d). These small changes, all within the uncertainty in the film dimensions and the positional accuracy of the stage, are enough to cause the absorptance peak to be smaller, broader and at a different position on the temperature axis from the peaks for nominal dimensions.

The significance of the peak, regardless of where on the temperature axis it is located, is that it will lead to a "temperature amplification" condition during the heating of the cantilever surface. On the leading edge of the absorptance peak, increases in temperature will cause increased absorption of laser power, which in turn cause further increases in temperature. The temperature is thus amplified in the vicinity of the absorptance peak until the temperature is high enough to surpass the peak, where absorptance decreases with temperature, and equilibrium can be attained. Thus, the presence of this region in the absorptance profile can explain the temperature jump observed in the peak temperature versus power curve in Fig. 5.

Another important consequence that the non-linear absorptance profile will have on the thermal behavior of the laser-heated cantilever is that the absorption of laser energy will not be uniform across the heated surface. This creates the possibility for regions of the heated surface to have lower absorptance at a higher temperature than other regions, such that the temperature distribution on the surface will not be solely dependent on the profile of the heating laser beam, but rather upon the product of the profile and the absorptance distribution on the surface. For a quasi-Gaussian laser profile as used in this study, a lower absorptance at a higher temperature (e.g. $T > 350\,^{\circ}\mathrm{C}$) can lead to a more uniform power deposition on the laser-heated surface, which can drive the system towards equilibrium much faster than if the absorbed laser power were simply proportional to the input laser power. This issue will be discussed in more detail in the following section.

5. Thermal modeling

As mentioned previously, temperature measurements of laser-heated cantilevers showed a linear increase in peak temperature for laser powers less than 320 mW and then a non-linear increase in peak temperature when the power approaches 440 mW (cf. Fig. 5). The peak temperature experiences a jump from around 120 °C to approximately 400 °C between 415 and 440 mW. Therefore, the primary objective of the heat transfer model is to investigate the impact of the absorptance model described previously on the temperature distribution in a polysilicon microcantilever and explain the observed abrupt increase in peak temperature with laser power.

In order to calculate the initial transient response and final steady-state temperature distribution in the microcantilever, a two-dimensional, explicit, finite difference model was developed. One of the primary assumptions of this model is that any temperature variation through the thickness of the cantilever is negligible, allowing the use of a two-dimensional model. While convection from the top and bottom surfaces of the cantilever will create a slight variation in temperature through the cantilever, the structure is over 200 times longer and over 100 times wider than it is thick. Consequently, as shown by Rogers and Phinney [20], any transient temperature gradients through the thickness equilibrate at rates that are 4–5 orders of magnitude faster than the heat transfer along the length or width and the steady-state gradient in this direction is much smaller than the gradient in the other two directions.

Given that it is reasonable to assume a two-dimensional model for the temperature distribution, the governing heat diffusion equation is

$$\frac{\partial}{\partial x}\left(k\frac{\partial T}{\partial x}\right)+\frac{\partial}{\partial y}\left(k\frac{\partial T}{\partial y}\right)+S=C\frac{\partial T}{\partial t} \tag{3}$$

where k is the thermal conductivity, T is the temperature, x is the distance along the cantilever length, y is the distance along the width of the cantilever, S is a source term that accounts for the energy generation from the laser, C is the heat capacity per unit volume, and t is time. This equation requires two boundary conditions in the x-direction, two in the y-direction, and an initial condition. Before being irradiated by the laser, the initial condition of the cantilever is a uniform temperature of 30 °C at $t = 0$. For the boundaries in the y-direction and for the boundary at the tip ($x = L$) of the cantilever, the conduction into the boundary is equated to the convection leaving the boundary. The specifics of modeling the convection losses for this microscale system are described later. The temperature at the anchor of the cantilever ($x = 0$), is assumed to be equal to the temperature of the underlying substrate. For this assumption to be true, excellent thermal contact between the cantilever and substrate must exist. Unfortunately, multiple layers of polysilicon and SiO_2 exist between the cantilever and substrate resulting in decreased conduction and an elevated anchor temperature especially when the maximum temperature in the cantilever is hundreds of degrees more than the underlying substrate. However, the modeling of the conduction in this anchor region is beyond the scope of this work, so using experimental observations (cf. Figs. 3a and 4), the anchor boundary temperature is set to 30 °C if the maximum temperature in the cantilever is less than 300 °C, but at an elevated temperature of 45 °C if the maximum temperature is greater than 300 °C.

Using a forward-time-centered-space (FTCS) finite difference scheme with equal spatial steps between nodes (i.e. $\Delta x = \Delta y$), the finite difference equation for an inner node m, n at a subsequent time step $p + 1$ is

$$T_{m,n}^{P+1} = Fo\left(T_{m-1,n}^{P} + T_{m+1,n}^{P} + T_{m,n-1}^{P} + T_{m,n+1}^{P}\right) + \frac{S\Delta t}{Cz} + \frac{h\Delta t}{Cz}T_{\infty} + \left(1 - 4Fo - \frac{h\Delta t}{Cz}\right)T_{m,n}^{P} \quad (4)$$

where z is the thickness of the cantilever, Δt is the time step, h is the heat transfer coefficient, T_∞ is the air temperature, and Fo is the Fourier number which is defined as

$$Fo = \frac{k\Delta t}{C(\Delta x)^2} \quad (5)$$

The laser source term, S, is defined as

$$S = \alpha I \quad (6)$$

where α is the absorptance coefficient determined using the optical model presented previously and I is the incident laser intensity. Measurement of the laser output results in an elliptical beam that is best fit by a modified-Gaussian profile of the form

$$I = I_0 \exp\left(-2\frac{(x - x_0)^4}{w_x^4}\right)\exp\left(-2\frac{(y - y_0)^4}{w_y^4}\right) \quad (7)$$

where I_0 is the peak intensity at the center of the beam (x_0, y_0), x and y are distances from the center of the beam, and w_x and w_y are the beam $1/e^2$ radii in the x- and y-directions, which were found to be 137 μm and 69 μm, respectively,[1] corresponding to the full width half maximum (FWHM) values of 210 μm and 106 μm of the experiment.

5.1. Thermophysical properties and parameters

The heat capacity per unit volume used throughout this study was taken to be a constant 1.7 MJ/m^3 K [21]. While the heat capacity is temperature dependent, the variation for the temperatures in this study is small enough to be neglected. However, the temperature dependence of the thermal conductivity is quite significant for the temperature range studied and was included. Given the nature of MEMS fabrication, all thermophysical properties including the thermal conductivity can vary from process to process and run to run. Consequently, it is important to use thermal conductivity measurements from films that were fabricated in a similar manner to those being studied. The temperature dependant thermal conductivity measurements for this study were taken on SUMMiT Poly4 layers and should provide an accurate prediction. From these measurements, the thermal conductivity in W/m·K can be calculated from the temperature, T, in K using [22]

$$k = 5859T^{-0.008139} - 5535. \quad (8)$$

The final thermophysical parameter required for the model is the heat transfer coefficient, h. In a macroscale system, the value of h may be approximated using free convection correlations based on the Rayleigh number. However, these correlations are not valid for this microscale system where the Rayleigh number is on the order of 10^{-3}–10^{-2}. This minuscule Rayleigh number suggests that most of the energy lost from the cantilever is through conduction into the air and not through bulk fluid motion. Therefore, the energy loss from the beam was modeled strictly as conduction into the surrounding air although it will still be termed convection so not to be confused with the conduction within the cantilever.

Two different models were considered for modeling the convection. In the first, the air is modeled as a semi-infinite medium. One difficulty with this model is that a real boundary exists in the substrate approximately 10.75 μm below the bottom of the cantilever. So the alternative approach was to consider the air as a finite medium with a length equal to this 10.75 μm gap between cantilever and substrate. However, that might not accurately predict the losses from the top or sides of the cantilever since there is no real surface at this finite length. Consequently, the actual convection model combines these two ideas by incorporating a real surface 10.75 μm below the bottom of the cantilever and an imaginary surface at some distance L_{imag} from the top and side surfaces. Using this approach, the heat transfer coefficient from the top of the cantilever is given by

$$h = \frac{k_{air}}{t_{gap}}\left(1 + \frac{t_{gap}}{L_{imag}}\right) \quad (9)$$

where k_{air} is the temperature dependant thermal conductivity of air and t_{gap} is the 10.75 μm gap height between the bottom of cantilever and substrate. The value of L_{imag} was then used as a fitting parameter in the model. Eq. (9) is valid for an internal node. For nodes on the side of the cantilever or at a corner, the equation for h is adjusted due to the decreased area of these nodes although the change in h for these nodes is less than 2%.

Using this convection model, the best value for L_{imag} was found by running the model with a laser power of 532 mW in order to compare the temperature distribution found using the model to the experiments at this laser power (Fig. 4). The strategy for finding the best value of L_{imag} was to choose it such that the peak temperature at the center of the cantilever and the temperature at the tip of the cantilever were consistent with the experimental measurements. By comparing the temperatures at the tip, one can best observe the effect of convection since this is the primary heat loss mechanism in that portion of the cantilever. This turned out to be an effective strategy because the best value for L_{imag} was fairly uniform for the different absorptance profiles. Whatever absorptance profile is used, a value of L_{imag} less than 108 μm, results in a suppressed tip temperature suggesting too much convection loss. Therefore, a value of $L_{imag} = 108$ μm will be used throughout *all* of the model calculations. Due to the temperature dependence of the

[1] The $1/e^2$ radius is related to the FWHM spot size reported in Section 1 through $w_{x/y} = 0.652\text{FWHM}_{x/y}$.

thermal conductivity of air, the resulting value of h varies from around 2500 W/(m^2 K) at 25 °C to 5500 W/(m^2 K) at 450 °C. Since bulk fluid motion has been neglected in the derivation of Eq. (9) resulting in a heat transfer coefficient that is primarily affected by the thermal conductivity of air, the applicability of Eq. (9) is limited to cases where the Rayleigh number is much less than unity.

In order to confirm the accuracy of the model, an exact analytical solution for an extended surface was used. To best simulate the actual experimental conditions while still allowing for an analytical solution, the laser radiation was simplified to a uniform heat flux at the top surface of the cantilever. Further simplifications included a constant thermal conductivity, k, and a constant heat transfer coefficient, h. The model proves to be highly accurate with an R^2 value of 0.9999 when compared to the analytical solution for a grid spacing of 10 μm in both the x- and y-directions with a time step of 0.3 μs.

The effect of grid spacing on the accuracy of the model was investigated by comparing model results to the analytical solution for several grid spacings. In each case, the time-step was adjusted to produce comparable Fourier numbers for the different cases. Courser grids of 50 and 25 μm led to R^2 values of 0.9983 and 0.9980, respectively. The accuracy of the code then improved for grids with spacing of 12.5 and 10 μm, which both had R^2 values better than 0.9996.

5.2. Model results

The primary objective in developing this model was to accurately predict the steady-state temperature distribution in a microcantilever irradiated by a laser with a secondary objective of understanding the amplification of peak temperature for a relatively small increase in laser power between 415 and 440 mW. The speed at which the system reaches steady state for different laser powers is also of interest.

As discussed previously, small changes in optical properties or incident laser angle have a significant impact on the temperature-dependent absorptance of the cantilever. When the absorptance profiles shown in Fig. 8 for nominal thicknesses and gaps were used in the model, the predicted temperatures in the microcantilever were too high at both laser powers, 314 and 532 mW. However, by using these absorptance profiles along with numerous others generated using the LTR method, useful observations could be made concerning the influence of the location of the absorptance peak and the overall magnitude of the absorptance. From these observations, an optical absorptance profile was generated that creates the best fit between the experimental temperature profiles and thermal model. The resulting absorption profile is shown by the closed symbols in Fig. 8. Note that this "adjusted" profile is similar to the one obtained for LTR calculations with non-nominal thicknesses and gaps (Fig. 8, open symbols) and is plausible given the uncertainties in device thicknesses and assumed temperature dependencies.

The fact that this absorptance profile was generated by comparing the thermal model, which includes a "best-fit" convection relationship, to experimental values is an obvious concern. However, the convection relationship has little effect on the overall observations noted for the optical absorptance data and as previously mentioned, the absorptance profile used had little influence on the convection relationship so while not completely independent, their effect is independent enough that each can be considered to be unique.

Fig. 3a shows the temperature distribution along the length of the cantilever predicted by the finite difference model compared to the distribution observed in the experiments for a laser power of 314 mW, which is below the power where the jump in temperature occurs. The solid line in the figure is the model prediction while the diamonds show the experimental results. The model fits the data extremely well with an $R^2 = 0.9634$. At this same laser power, the temperature distribution along the width of the cantilever was also compared to the experimental results (Fig. 3b). Again, the model does an excellent job of predicting the temperature distribution.

To further compare the model and experimental results, Fig. 4 depicts the same comparison between model and experiment as in Fig. 3 but for a laser power of 532 mW which constitutes a power above the amplification in peak temperature. Again, qualita-

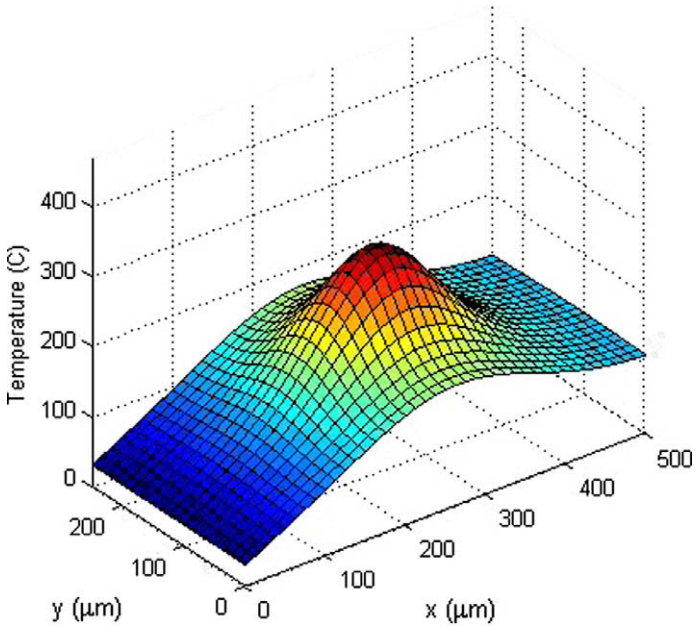

Fig. 9. Spike in temperature at the center of the cantilever (main) observed in the numerical modeling of the cantilever during transient heating. The location spike coincides with a spike in absorbed laser intensity (Fig. 10a). The laser power used in this simulation was 532 mW and the image shown corresponds to the maximum peak absorbed intensity which occurs approximately 1.8 ms after the initiation of heating.

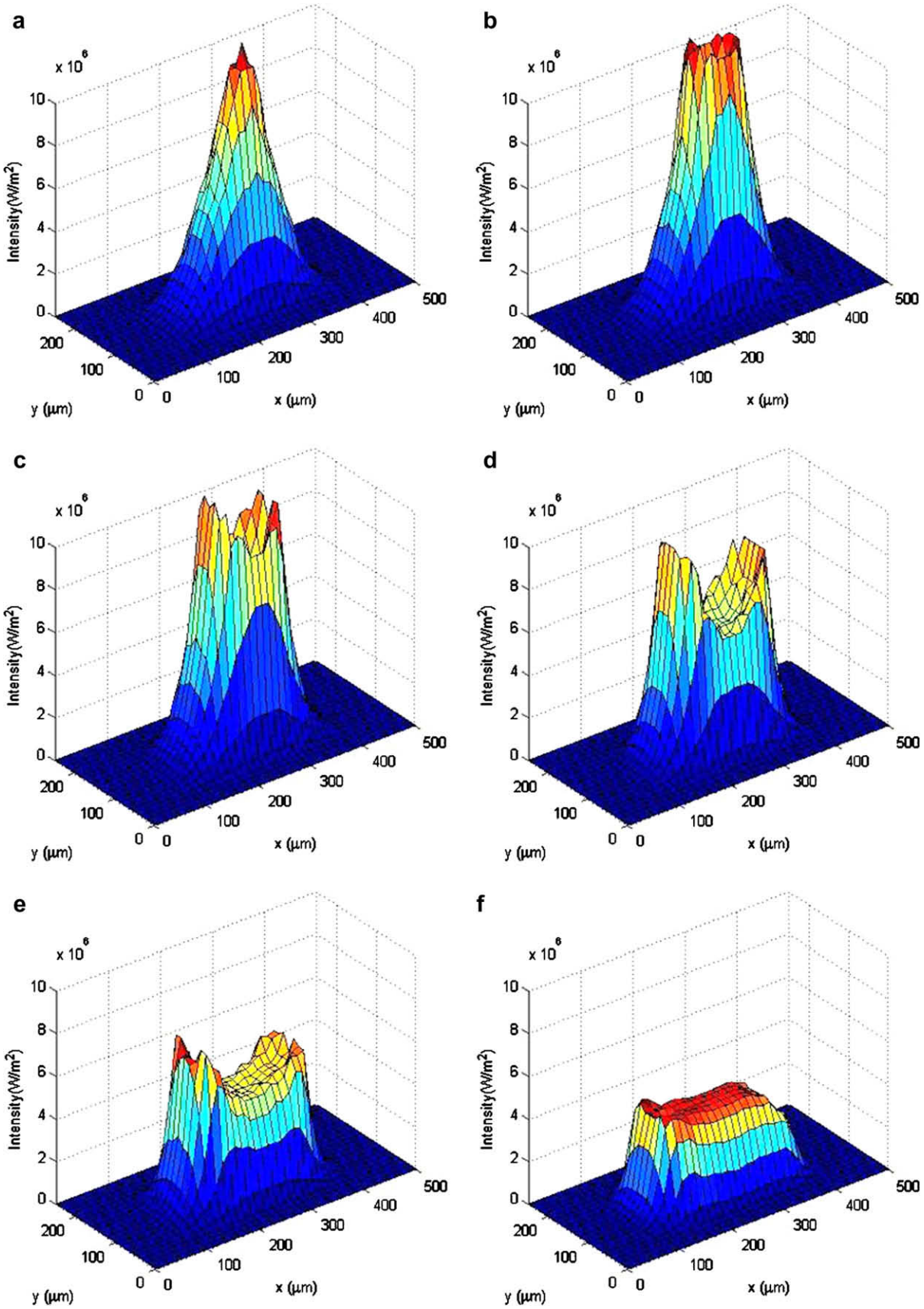

Fig. 10. The absorbed laser intensity shown in the inset of Fig. 9 for a laser power of 532 mW is shown at different times during laser heating. After the spike in absorbed laser intensity appears in the center of the irradiation area (a), the absorption peak moves outward (b–e), and the absorbed laser intensity becomes nearly uniform across the spot (f). The time between the peak (a) and the steady-state profile (f) is approximately 1.7 ms.

tive agreement between model and experiment is generally good but the R^2 value (0.9134) for this case is a little lower than for the lower laser power. Qualitatively, the temperature distribution follows the experimental data fairly well but the model curve distribution is too broad. Possibilities for this include too much conduction out of the hotter regions suggesting that the thermal conductivity may be too high, an absorptance profile that is too broad causing too much energy to be absorbed in the hotter regions, or an incident laser profile that is too broad.

In order to compare the amount of energy conducted into the underlying substrate to that which is transferred via convection into air, the model was used to quantify the magnitude of each mode under steady-state conditions. From these simulations, convection is the dominant mode of heat transfer accounting for 60–70% of the energy transfer out of the cantilever with the higher proportion occurring at higher laser powers. While this proportion is high when one compares the thermal conductivity of the polysilicon cantilever to air, the surface area of the cantilever over which convection occurs is approximately 450 times larger than the cross-sectional area at the cantilever anchor.

Since an objective of the model is to illustrate why a non-linear jump in temperature of over 200 °C occurs between laser powers of 415 and 440 mW, the peak temperature predicted by the model was compared to the peak temperature measured for a range of laser powers. The results are shown in Fig. 5. Excellent agreement is observed between the model and the experimental results, with the model predicting a jump in peak temperature from 175 to 413 °C with a power increase of just 5 mW from 420 to 425 mW, which is consistent with the experimental observations.

As one might expect, this amplification in peak temperature is directly related to the peak in absorptance. Two-dimensional plots of the transient temperature distribution were synchronized with two-dimensional plots of the transient absorbed laser intensity, which combine the temperature-dependent absorptance data with the modified-Gaussian laser profile. It was observed that as the cantilever is initially heated by the laser, the absorbed intensity fits the modified-Gaussian profile of the incident beam. However, as the temperature of the center of the cantilever reaches the temperature where the peak absorption occurs, the absorbed intensity in this region spikes creating a spike in temperature as shown in Fig. 9. Then as the temperature in this region moves past where the absorptance peak occurs, the spike in absorbed intensity moves outward from the center of the laser spot like a wave, after which the absorbed intensity becomes almost uniform, "top-hat", across the spot as shown in Fig. 10. The uniformity of the absorbed laser intensity causes the system to reach steady-state more quickly than if the absorbed intensity profile was still a Gaussian profile. In fact, the model predicts that a cantilever heated at a laser power of 314 mW, (Fig. 3) will reach steady-state in 5.5 ms while a cantilever heated with 532 mW of laser power (Fig. 4) reaches steady state in 4.5 ms.

The results obtained thus far reinforce the importance of considering coupled optical-thermal effects in the design phase of optical microsystems. For the approach presented here to be truly useful for device design, however, refinements are needed. Experimental validation of the model used for the thermal transport into the air for a heated SUMMiT™V structure would be beneficial. Additionally, improvements to the optical absorptance modeling requires improved determination of both layer thicknesses and temperature-dependent optical properties, which are presently not known with sufficient accuracy to provide a direct correlation between the measurements and the model. Obtaining accurate knowledge of these optical and thermal parameters *a priori* will extend the benefit of the model from a discovery platform into an enabling and predictive simulation platform.

6. Conclusions

The thermal response of polycrystalline silicon microcantilevers due to laser irradiation depends on the absorption of laser energy and transport of thermal energy. Temperature measurements were made on surface-micromachined polysilicon microcantilevers that are nominally 500 μm long, 250 μm wide, and 2.25 μm thick using Raman thermometry. Temperature profiles showed maximum temperatures in the center of the irradiated region of ~115 °C at 314 mW and ~460 °C at 532 mW with ±4 °C uncertainty in the temperatures. Measurements of peak temperature versus laser power revealed a significant increase in peak temperature of over 200 °C for a small increase in laser power from 415 to 440 mW.

Since polysilicon is semitransparent at a laser wavelength of 808 nm, the absorption of laser energy in the polysilicon microcantilevers depends on the thicknesses of the layers and gaps, the polysilicon temperature, and the irradiation angle. A modular technique adapted from the LTR method of Mazilu et al. [19] was used to calculate the absorptance versus temperature curves for polysilicon. These calculations revealed a peak in absorptance which results in a temperature amplification as the microcantilever is heated.

A two-dimensional, finite difference model calculated the thermal response for polysilicon microcantilevers. The energy loss to the environment was determined by matching the temperature profile for a polysilicon cantilever heated by 808 nm at 532 mW. An optical absorptance profile for the model was obtained that is similar to those from the LTR calculations. The predicted temperatures compare very well with the measured temperatures for the temperature profiles at 314 and 532 mW as well as the peak temperatures versus laser power values for laser powers up to 719 mW. Calculations of the absorbed laser intensity confirm the effect of the temperature on the optical properties and the amplification of the optical absorption leading then to amplification in the peak temperature when near a peak in absorptance as a function of temperature. Temperature-dependent optical properties need to be accurately known and used in models in order to make reasonable predictions of the thermal performance and likelihood of failure for microsystems irradiated by lasers.

Acknowledgments

Sandia is a multiprogram laboratory operated by Sandia Corporation, a Lockheed Martin Company, for the United States Department of Energy's National Nuclear Security Administration under Contract DE-AC04-94AL85000. The authors acknowledge the assistance of Wayne Trott, Jaime Castaneda, and Allen Gorby during the experimental measurements.

References

[1] D.M. Burns, V.M. Bright, Optical power induced damage to microelectromechanical mirrors, Sensors Actuators A 70 (1-2) (1998) 6–14.
[2] L.M. Phinney, J.R. Serrano, Influence of target design on the damage threshold for optically powered MEMS thermal actuators, Sensors Actuators A 134 (2) (2007) 538–543.
[3] X. Xue, S.B. Koppaka, L.M. Phinney, T.J. Mackin, Effects of laser irradiation on the surface topology of surface-micromachined polysilicon structures, in: Proceedings of the 2004 SEM X International Congress and Exposition on Experimental and Applied Mechanics, Paper No. 305, Society for Experimental Mechanics, Inc., Bethel, CT, 2004, pp. 1–7.
[4] C.R. Forest, P. Reynolds-Browne, O. Blum-Spahn, J. Harris, E. Novak, C.C. Wong, S. Mani, F. Peter, D. Adams, Static and dynamic optical metrology of micromirror thermal deformation, in: Proceedings of the 2004 Nanotechnology Conference and Trade Show, Boston, Massachusetts, 2004, pp. 1–4.
[5] A. Agarwal, S. Arney, B.P. Barber, S.G. Kosinski, J.D. LeGrange, V.R. Raju, R. Ruel, Laser power monitoring using MEMS micromirror technology, in: Proceedings

of the 1999 IEEE International Reliability Physics Symposium, Institute of Electrical and Electronics Engineers, Piscataway, NJ, 1999, pp. 198–201.
[6] J.R. Serrano, L.M. Phinney, Displacement and thermal performance of laser heated asymmetric MEMS actuators, J. Microelectromech. Syst. 17 (1) (2008) 166–174.
[7] C.-N.C. Wong, S. Graham, Investigating the thermal response of a micro-optical shutter, IEEE Trans. Component Packaging Technol. 26 (2) (2003) 324–331.
[8] L.M. Phinney, O.B. Spahn, C.C. Wong, Experimental and computational study on laser heating of surface micromachined cantilevers, in: D.M. Tanner, R. Ramesham (Eds.), Proceedings of SPIE: Reliability, Packaging, Testing and Characterization of MEMS/MOEMS V, vol. 6111, Society of Photo-Optical Instrumentation Engineers, Bellingham, WA, 2006, pp. 1–7.
[9] L.M. Phinney, J.W. Rogers, Pulsed laser repair of adhered surface-micromachined polycrystalline silicon cantilevers, J. Adhes. Sci. Technol. 17 (4) (2003) 603–622.
[10] J.R. Serrano, L. M. Phinney, Micro-Raman thermometry of laser heated surfaces, in: Proceedings of InterPACK'07, IPACK2007-33571, American Society of Mechanical Engineers, New York, NY, 2007, pp. 1–7.
[11] J.J. Sniegowski, M.P. de Boer, IC-Compatible polysilicon surface micromachining, Annu. Rev. Mater. Sci. 30 (2000) 299–333.
[12] R. Tsu, J.G. Hernandez, Temperature dependence of silicon Raman lines, Appl. Phys. Lett. 41 (11) (1982) 1016–1018.
[13] M. Balkanski, R.F. Wallis, E. Haro, Anharmonic effects in light scattering due to optical phonons in silicon, Phys. Rev. B 28 (4) (1983) 1928–1934.
[14] T. Beechem, S. Graham, S.P. Kearney, L.M. Phinney, J.R. Serrano, Invited article: simultaneous mapping of temperature and stress in microdevices using micro-Raman spectroscopy, Rev. Sci. Instrum. 78 (6) (2007). 061301-1-9.
[15] S.P. Kearney, L.M. Phinney, M.S. Baker, Spatially resolved temperature mapping of electrothermal actuators by surface Raman scattering, J. Microelectromech. Syst. 15 (2) (2006) 314–321.
[16] J.R. Serrano, L.M. Phinney, S.P. Kearney, Micro-Raman thermometry of thermal flexure actuators, J. Micromech. Microeng. 16 (7) (2006) 1128–1134.
[17] X. Xu, C.P. Grigoropoulos, High temperature radiative properties of thin polysilicon films at the $\lambda = 0.6328$ μm wavelength, Int. J. Heat Mass Transfer 36 (17) (1993) 4163–4172.
[18] G.E. Jellison Jr., F.A. Modine, Optical functions of silicon between 1.7 and 4.7 eV at elevated temperatures, Phys. Rev. B 27 (12) (1983) 7466–7472.
[19] M. Mazilu, A. Miller, V.T. Donchev, Modular method for calculation of transmission and reflection in mulitlayered structures, Appl. Opt. 40 (36) (2001) 6670–6676.
[20] J.W. Rogers, L.M. Phinney, Temperature response of silicon MEMS cantilevers during and after Nd:YAG laser irradiation, Numer. Heat Transfer A 45 (8) (2004) 737–750.
[21] A.D. McConnell, U. Srinivasan, K.E. Goodson, Thermal conductivity of doped polysilicon layers, J. Microelectromech. Syst. 10 (3) (2001) 360–369.
[22] L.M. Phinney, J.D. Kuppers, R.C. Clemens, Thermal conductivity of SUMMiT™V polycrystalline silicon report, SAND2006-7122, Sandia National Laboratories, Albuquerque, NM, November 2006.